

Quantum colored strings in the hole-doped t - J_z model

Jia-Long Wang,¹ Shi-Jie Hu,^{1,2,*} and Xue-Feng Zhang^{3,4,†}

¹Beijing Computational Science Research Center, Beijing 100193, People's Republic of China

²Department of Physics, Beijing Normal University, Beijing 100875, People's Republic of China

³Department of Physics and Chongqing Key Laboratory for Strongly Coupled Physics, Chongqing University, Chongqing 401331, China

⁴Center of Quantum Materials and Devices, Chongqing University, Chongqing 401331, China

The stripe phase, an intertwined order observed in high-temperature superconductors, is regarded as playing a key role in elucidating the underlying mechanism of superconductivity, especially in cuprates. Following Jan Zaanen's early scenario, the full-filled charge stripe can be taken as the interactive elastic quantum strings of holes, stabilized by π -phase shifts between neighboring magnetic domains. However, this scenario is challenging to explain, particularly in terms of electron pairing, which necessitates hole pairs. In this work, we propose a new effective model for describing the stripe phase in the hole-doped t - J_z model. With respect to the antiferromagnetic background, the model comprises three types of color-labeled point-defects coupling to an effective spin field. Comparing with numerical results from large-scale density matrix renormalization group (DMRG) simulations, we find semi-quantitative agreement in local hole density, magnetic moment, and the newly proposed spectrum features of the effective spin field. By systematically analyzing the hole-density distribution and the scaling of groundstate energy at different system sizes, we determine the effective core radius and the effective hopping amplitude of the quantum string. Furthermore, the local pinning field can be finely adjusted to drag the quantum string, offering a potential method for detecting it in optical lattices.

I. INTRODUCTION

Decoding the mechanism of the high- T_c superconductivity is one of the central tasks of condensed matter physics, also posing a challenge for the whole field of physics [1, 2]. Recent numerous numerical simulations of the Hubbard model [3–5], the t - J model [6, 7], and their extensions [8–12] have underscored the potential significance of the stripe phase [12–14]. This phase, observed prominently in the underdoped region, arises from the doping holes into the Mott insulator that hosts antiferromagnetic (AF) order [15–18]. Then, the introduction of π -phase shifts between magnetic domains can lead to the stable emergence of one-dimensional (1D) topological defects, or strings [19, 20].

Strings widely exist in the frustrated magnetic system [21]. Because of the off-diagonal interactions, the string appears to behave in a “quantum” manner, which means that the string becomes a worldsheet in the 2+1 dimensions [18]. The complicated interplay among these strings renders extremely unconventional quantum phases, including the deconfined quantum phase transition [22–24], quantum string Luttinger liquid [25, 26], emergent RK point [27], and others [28, 29]. These phenomena can be effectively described by a spin-1/2 chain within the framework of the effective theory [21, 22, 26, 29]. Meanwhile, the quantum string can also be understood *via* generalized symmetry [30] and its relationship to the 1-form charge with $d-1$ co-dimensions [31, 32]. Then, it would be straightforward to consider the possibility of an effective description of the string in the stripe phase.

In this work, we consider the t - J_z model, which contains the minimal ingredients required for the stripe phase to emerge as its ground state. Due to the absence of intricate spin-flipping processes between nearest neighboring (NN) sites, we

have been able to construct an effective theory capable of describing the quantum string. To validate this model, we employed the two-dimensional (2D) density matrix renormalization group (DMRG) method, comparing its results with exact diagonalization of the effective model (EM). At last, we demonstrate that a tiny pinning field can be used to manipulate the quantum string. The paper is structured as follows: Sec. II elaborates the t - J_z model, Sec. III introduces the effective model, Sec. IV compares the DMRG results with those from the effective model, and finally, Sec. V presents our conclusion.

II. t - J_z MODEL

The Hamiltonian of the t - J_z model loading on a cylinder of $L_x \times L_y$ square lattices can be simplified and written as follows:

$$H = -t \sum_{\langle i,j \rangle} \sum_{\sigma} (f_{i,\sigma}^{\dagger} f_{j,\sigma} + \text{h.c.}) - \frac{J_z}{2} \sum_{\langle i,j \rangle} \sum_{\sigma} n_{i,\sigma} n_{j,\bar{\sigma}}, \quad (1)$$

where $f_{i,\sigma}^{\dagger}$, $f_{i,\sigma}$ and $n_{i,\sigma} = f_{i,\sigma}^{\dagger} f_{i,\sigma}$ represent the creation, annihilation and density operator of the fermion with the spin polarization $\sigma = \uparrow, \downarrow$ along the z -axis, respectively. $\bar{\sigma}$ is the reverse of the σ . t denotes the coefficient of the hoppings between two NN sites labeled as the bond $\langle i, j \rangle$, and J_z gives the magnitude of the Ising-type interactions. Hereafter, $t = 1$ sets the energy unit. L_x and L_y represent the length and the circumference of the cylinder, respectively. The coordinate of site- i is given by (x_i, y_i) , where $x_i = 1, \dots, L_x$ and $y_i = 1, \dots, L_y$. If necessary, we will change the index labels of the sites in the following discussion, e.g., $n_{i,\sigma} \equiv n_{\sigma}(x_i, y_i)$. The boundary condition of the cylinders is periodic (PBC) in the y -axis while open (OBC) in the x -axis. The lattice sites are arranged in one-dimensional (1D) path, with the coordinates $(x, y) = (L_x, 1), \dots, (1, 1), (L_x, 2), \dots, (1, 2), \dots$. The

* Corresponding author: shijiehu@csrc.ac.cn

† Corresponding author: zhangxf@cqu.edu.cn

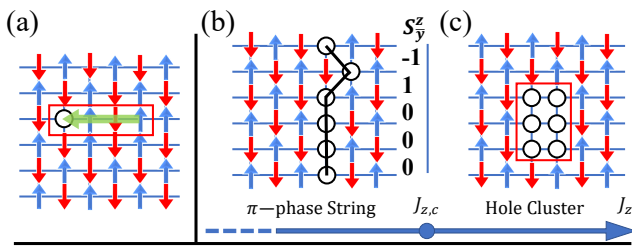


FIG. 1. Schematic pictures of (a) the Nagaoka mechanism, (b) a configuration of Zaanen's π -phase string (black line) and its spin-1 representation, and (c) the block cluster of holes (enclosed by a red rectangle) in the large- J_z limit. The hole (black circle) move in the AF background consisting of spin-up (blue arrow) and down (red arrow). The transition from the block cluster state to the π -phase string state happens at $J_{z,c}$ (blue dot).

number of lattice sites $N = L_x L_y$ is also defined. For a single string, we always choose the filling number of holes $N^{(h)} = L_y$ with respect to the AF background.

When a single hole is doped into the AF background, it can move to another site through the hopping process. However, as demonstrated in Fig. 1(a), the creation of ferromagnetic bonds coincide with the breaking of AF bonds along the path of the hole, resulting in an energy cost proportional to the path length. This confinement of the hole by the AF background is usually known as the Nagaoka mechanism [33, 34].

However, recent studies on the Hubbard model and the t - J model [3–6, 8–10] have shown that holes can induce the stripe phase, characterized by the stable presence of a π -phase shift between two neighboring magnetic domains. According to Jan Zaanen's scenario, these holes collectively form an elastic quantum string, depicted in Fig. 1(b). Consequently, the incommensurate magnetic order observed in experiments can be attributed to the effective repulsive interaction between strings [18]. In the following section, we will review Zaanen's string model as a primer before discussing the novel colored string (CS) model.

III. EFFECTIVE THEORY

A. Zaanen's string

When J_z dominates, L_y holes doped into the AF background tend to stay together to minimize potential energy dictated by the J_z -terms in the model (1). As illustrated in Fig. 1(c), they form a block cluster with the largest number of adhering AF bonds. Conversely, when t is significant, collective hole motion is absent. In the intermediate region, a string can survive in the ground state, thereby separating the whole system into two AF domains [19]. Subject to the topological constraint, two domains exhibit either a 0 or π -phase shift, with the string identified as a 0-phase or π -phase string, respectively. As shown in Fig. 1(b), the π -phase string can vibrate more readily through hole hopping and has lower energy compared to the 0-phase string. In our study, we only consider the low-energy π -phase string, simply referred to as the string.

The block cluster of holes transitions into a state with a string when the gained vibrational energy is sufficient to compensate for the loss of the potential energy [19]. For $L_y = 6$, the transition occurs at $J_{z,c} \approx 3.85$ (App. 1).

As with the string in frustrated magnetism [21, 22, 26, 29], the dynamics of the string can be effectively described by the spin-1 chain under the assumption that row- y has a single hole located at $X_y^{(h)}$. Specifically, we define a spin operator $S_{\bar{y}}$ between neighboring row- y and row- $(y+1)$, comprising components $S_{\bar{y}}^+$, $S_{\bar{y}}^-$ and $S_{\bar{y}}^z$, which represent the spin-flipping-up and down operators as well as the z -axis polarization, respectively. Obviously, $\bar{y} = y + 1/2$ modulo L_y . When the x -coordinates of the holes in these two rows are the same, that is, $X_y^{(h)} = X_{y+1}^{(h)}$, the configuration corresponds to $\uparrow\downarrow$ and is represented by a non-magnetic state $|S_{\bar{y}}^z = 0\rangle \equiv |0_{\bar{y}}\rangle$, as shown in Fig. 1(b). Therefore, the straight string along the y -axis corresponds to the state $|0_{1/2}0_{3/2}\cdots0_{L_y-1/2}\rangle$. Similarly, we can map the configuration $\downarrow\uparrow$ to $|1_{\bar{y}}\rangle$, and $\uparrow\uparrow$ to $|(-1)_{\bar{y}}\rangle$. In Fig. 1(b), the hole hopping processes mirror the effective spin-exchanging terms ($S_{\bar{y}}^+ S_{\bar{y}+1}^- + \text{h.c.}$). Additionally, both the configurations $|\pm 1\rangle$ violate an AF bond along the y -axis, resulting in a single-ion anisotropic term $(S_{\bar{y}}^z)^2$.

Overall, the effective spin-1 Hamiltonian is given by

$$H_e = -t \sum_y (S_{\bar{y}}^+ S_{\bar{y}+1}^- + \text{h.c.}) + \frac{J_z}{2} \sum_y (S_{\bar{y}}^z)^2.$$

where the ratio between J_z and t determines the ground state. Notably, the summation over y is equivalent to that over \bar{y} , with the former being the preferred choice in this study. Similar to the Haldane phase [35], $|\pm 1\rangle$ mark two point-like topological defects that cannot be annihilated *via* local operation. They serve as the 0-form topological charge on the 1-form string [36]. However, Zaanen's string is so simple that some interesting processes are lost, e.g., the electron pairing.

B. Colored string

The fundamental unit of Zaanen's string is the π -phase holon ($\uparrow\downarrow$ and $\downarrow\uparrow$). However, with the allowance of the hole hoppings along the y -axis, both the spinon ($\uparrow\downarrow\uparrow$ and $\downarrow\uparrow\downarrow$) and the dual-hole ($\uparrow\circ\uparrow$ and $\downarrow\circ\downarrow$) emerge. For simplicity, we use the colors $c = \mathbf{r}, \mathbf{g},$ and \mathbf{b} to label the spinon, holon, and dual-hole, respectively, and refer to them as *color particles* (CP). Thus, the annihilation (creation) operators for these particles at row- y are denoted as $r_y, g_y,$ and b_y ($r_y^\dagger, g_y^\dagger,$ and b_y^\dagger), using the mapping of *hardcore bosons*. Their density operators are given by $n_y^{(\mathbf{r})} = r_y^\dagger r_y, n_y^{(\mathbf{g})} = g_y^\dagger g_y$ and $n_y^{(\mathbf{b})} = b_y^\dagger b_y$. Moreover, we impose a constraint permitting only one CP in row- y : $\sum_c n_y^c = 1$, with the CP positioned at $x = X_y^{(\text{CP})}$. In particular, as the midpoint of the spinon \mathbf{r} and the dual-hole \mathbf{b} sit at the bond, we set the lattice spacing to 2 in this work, ensuring that the x -coordinates of CPs are integer. The *onsite* energy of CPs is only related to the process that describes the violation of the AF bonds in the x -axis, as outlined in Table. I.

Particle	Color	Configuration	Onsite energy
Spinon	r	$\uparrow\downarrow\uparrow$ and $\downarrow\uparrow\downarrow$	$J_z/2$
Holon	g	$\uparrow\circ\downarrow$ and $\downarrow\circ\uparrow$	J_z
Dual-hole	b	$\uparrow\circ\circ\uparrow$ and $\downarrow\circ\circ\downarrow$	$3J_z/2$

TABLE I. The onsite energy of CPs under consideration.

C. String vibration

The hole hopping along either the x -axis or y -axis changes the *filling status* of CPs in two adjacent rows. We begin by assuming that the location of the CP in row-1 is fixed, and then observe the vibration of the CS. For example, in the process

$$\mathbf{g-g} : \begin{array}{c} \uparrow \circ \downarrow \uparrow \\ \uparrow \downarrow \circ \uparrow \end{array} \implies \mathbf{r-b} : \begin{array}{c} \uparrow \circ \circ \uparrow \\ \uparrow \downarrow \downarrow \uparrow \end{array},$$

adjacent rows in the initial configuration on the left side are filled with two holons, forming a **g-g** pair, while in the final configuration on the right side, they contain a dual-hole and a spinon, forming an **r-b** pair. According to Table. I, we find that the transition from the **g-g** pair to the **r-b** pair does not entail any onsite energy cost.

The effective theory for hole hopping processes can be classified into two categories: (1) *diagonal interactions*, which are influenced by the distance between CPs, and (2) *off-diagonal interactions*, which deform the CS, produce the **r-b** pair, and move CPs along the CS. Then, it is obvious that the π -phase shift happens at the CP location in each row.

Diagonal interactions - The violation of the AF bonds along the y -axis results in the diagonal interaction among CPs. In Fig. 2(a), the displacement along the x -axis between the holons at row- y and row- $(y+1)$, i.e., $\mathcal{X}_{y+1}^{(\text{CP})} - \mathcal{X}_y^{(\text{CP})}$, can be represented as an effective *spin field* $\Gamma_{\bar{y}}^z \in \mathbb{Z}$ with integer values, where the absolute value $|\Gamma_{\bar{y}}^z|$ can exceed 1. After checking the violated AF bonds, indicated by the red links in Fig. 2, we clearly find that the energy loss is proportional to the distance $|\Gamma_{\bar{y}}^z|$. This means that configurations with larger distances have

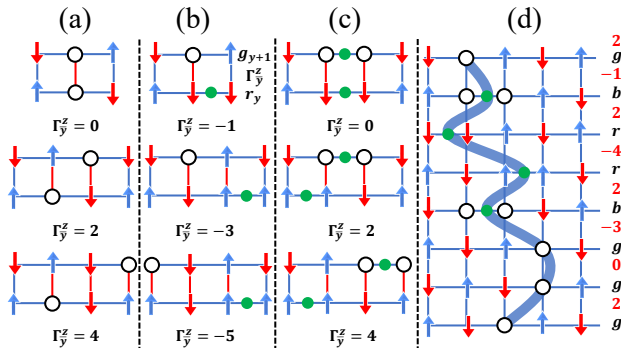


FIG. 2. Effective spin fields for showing the displacements between CPs for (a) $c_y - c_{y+1} = \mathbf{g-g}$, (b) **g-b**, and (c) **r-b**. A red link highlights a violated AF bond with an energy cost of $J_z/2$, and a green dot indicates the position of **r** or **b**. (d) A mapping of a cylinder configuration to a CS (blue line).

higher energy values and are thus significantly discouraged in the ground state, reminiscent of the Nagaoka mechanism. Then, the sign of $\Gamma_{\bar{y}}^z$ depends on the relative direction between CPs, and it does not affect the interaction. The same features can also be found in the interactions between different species of CPs, as demonstrated in Fig. 2(b,c).

In Fig. 2(d), the configuration of electrons in a cylinder can be mapped to a CS, which consists of three distinct species of CPs and is coupled to the effective spin field located at dual sites of the CS. After calculating all interactions listed in Table II, we can derive the diagonal energy of a CS, i.e.,

$$H_d = \sum_y \sum_{c,c'} V_{c,c'} \left(|\Gamma_{\bar{y}}^z| \right) n_y^{(c)} n_{y+1}^{(c')}.$$

Conf.: $c-c'$	$ \Gamma_{\bar{y}}^z $	$V_{c,c'}/J_z$	Conf.: $c-c'$	$ \Gamma_{\bar{y}}^z $	$V_{c,c'}/J_z$
g-g	$2\mathbb{N}$	$(\mathbb{N}+1)/2$	r-r	$2\mathbb{N}$	$\mathbb{N}/2$
r-g	$2\mathbb{N}+1$	$(\mathbb{N}+1)/2$	r-b	$2\mathbb{N}$	$(\mathbb{N}+1)/2^a$
g-b	$2\mathbb{N}+1$	$(\mathbb{N}+2)/2$	b-b	$2\mathbb{N}$	$(\mathbb{N}+2)/2$

^a When the natural number $\mathbb{N} = 0$, $V_{c,c'} = J_z$ does not follow the formula.

TABLE II. Strengths of non-zero diagonal interactions $V_{c,c'} \left(|\Gamma_{\bar{y}}^z| \right)$.

Off-diagonal interactions - The shape of the CS changes through the hopping processes of holes, which contributes to the vibrational energy. Same as Zaanen's string, when a hole in row- y hops to the left or the right, the effective spin fields in neighboring dual rows $(\bar{y}-1)$ and \bar{y} change as well, as shown in Fig. 3(a). Defining the "shift operator" $\Gamma_{\bar{y}}^\pm$ ($\Gamma_{\bar{y}}^-$) which raises (lowers) spin field as $\Gamma_{\bar{y}}^\pm |\Gamma_{\bar{y}}^z\rangle = |\Gamma_{\bar{y}}^z \pm 1\rangle$, we can derive the

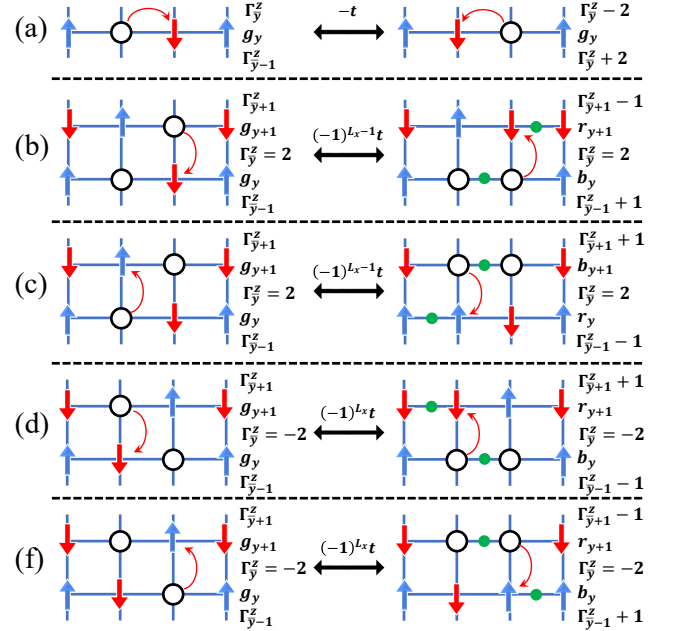


FIG. 3. Off-diagonal interactions update the configurations of CS via hole hoppings (red arrow) (a) along the x -axis, and (b-d) along the y -axis for the process **g-g** \implies **r-b** and reversion.

operator representation of the interaction, given by

$$H_o^{(g)} = -t \sum_y \left[\left(\Gamma_{\bar{y}}^+ \right)^2 n_y^{(g)} \left(\Gamma_{\bar{y}-1}^- \right)^2 + \text{h.c.} \right]. \quad (2)$$

Then, we can establish a connection with Zaanen's string by noting that the spin field reduces to the one for the spin-1 through the relations $\left(\Gamma_{\bar{y}}^\pm \right)^2 \leftrightarrow S_{\bar{y}}^\pm$ and $\Gamma_{\bar{y}}^z \leftrightarrow 2S_{\bar{y}}^z$.

In contrast, the hopping processes of holes along the y -axis bring about more complex changes to the CS. For instance, referring to Fig. 3(b-f), when the spin field $\Gamma_{\bar{y}}^z$ between \mathbf{g} - \mathbf{g} equal to ± 2 , they can transform to the \mathbf{r} - \mathbf{b} pair. Interestingly, the spin field in the middle remains unaffected, whereas the upper and lower ones alter through a form of spin exchange interaction. Then, the sign of the transition amplitude depends on the sign of the spin field $\Gamma_{\bar{y}}^z$, behaving akin to a gauge field. The corresponding Hamiltonian for $\Gamma_{\bar{y}}^z = \pm 2$ can be explicitly written as

$$H_o^{(\mathbf{r}-\mathbf{b}/\mathbf{g}-\mathbf{g})} = \pm t \sum_y \left(\Gamma_{\bar{y}+1}^\mp r_{y+1}^\dagger b_y^\dagger \Gamma_{\bar{y}-1}^\pm + \Gamma_{\bar{y}+1}^\pm b_{y+1}^\dagger r_y^\dagger \Gamma_{\bar{y}-1}^\mp \right) g_{y+1} g_y.$$

Meanwhile, in Fig. 4, we find that the spinon and dual-hole can switch places with the holon when the corresponding middle spin field equal to $\Gamma_{\bar{y}}^z = \pm 1$ and ± 3 , respectively. The influence on the effective spin fields is the same type as the generation of the \mathbf{r} - \mathbf{b} pair. However, their sign of hopping is independent of $\Gamma_{\bar{y}}^z$ and the corresponding Hamiltonians are

$$H_o^{(\mathbf{r}-\mathbf{g}/\mathbf{g}-\mathbf{r})} = -t \sum_y \Gamma_{\bar{y}+1}^\mp r_{y+1}^\dagger r_y g_y^\dagger g_{y+1} \Gamma_{\bar{y}-1}^\pm, \quad \Gamma_{\bar{y}}^z = \pm 1.$$

$$H_o^{(\mathbf{b}-\mathbf{g}/\mathbf{g}-\mathbf{b})} = -t \sum_y \Gamma_{\bar{y}+1}^\pm b_{y+1}^\dagger b_y g_y^\dagger g_{y+1} \Gamma_{\bar{y}-1}^\mp, \quad \Gamma_{\bar{y}}^z = \pm 3.$$

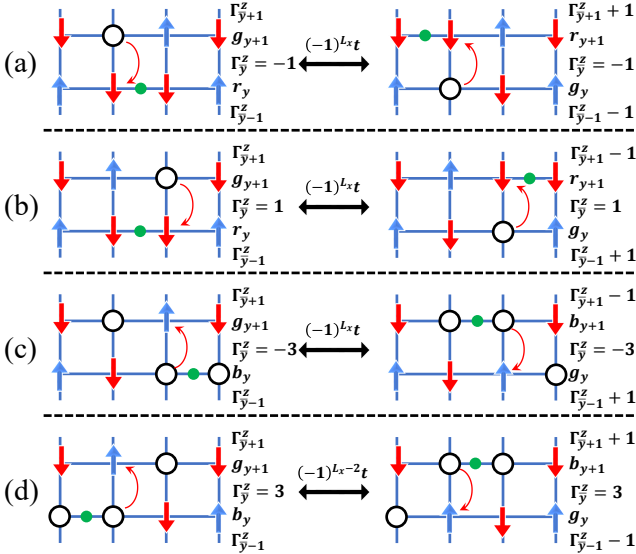


FIG. 4. Other off-diagonal interactions update the configurations of CS via hole hoppings (red arrow) for the processes (a,b) \mathbf{r} - $\mathbf{g} \Rightarrow \mathbf{g}$ - \mathbf{r} , and (c,d) \mathbf{b} - $\mathbf{g} \Rightarrow \mathbf{g}$ - \mathbf{b} .

Overall, the diagonal interactions limit the displacement between CPs, while the off-diagonal interactions both deform the CS and enable the motion of the spinons and dual-holes along the CS, all of which are summarized as the full Hamiltonian of the effective model of CS:

$$H_e^{\text{CS}} = H_d + \left(H_o^{(g)} + H_o^{(\mathbf{r}-\mathbf{b}/\mathbf{g}-\mathbf{g})} + H_o^{(\mathbf{r}-\mathbf{g}/\mathbf{g}-\mathbf{r})} + H_o^{(\mathbf{b}-\mathbf{g}/\mathbf{g}-\mathbf{b})} + \text{h.c.} \right). \quad (3)$$

D. Translation

After introducing a free CP in row-1, we can define the translation of the CS along the x -axis, as illustrated in Fig. 5(a,b). This allows CS to reach the leftmost or rightmost edges. To simplify, we utilize $\chi_1^{(\text{CP})}$ to mark the position $\chi^{(\text{CS})}$ of CS, that is, $\chi^{(\text{CS})} \equiv \chi_1^{(\text{CP})}$. The location of CP at any row can also be selected as $\chi^{(\text{CS})}$, which does not affect the conclusion. Definitely, the shift operator \mathcal{X}^\pm describes the movement of CS in accordance with the relationship $\mathcal{X}^\pm |\chi^{(\text{CS})}\rangle = |\chi^{(\text{CS})} \pm 1\rangle$. Then, the corresponding operator representation of process Fig. 5(a)→(b) changes from the term for row-1 in Eq. (2) into

$$-t \left[\left(\Gamma_{3/2}^+ \right)^2 n_1^{(g)} \mathcal{X}^- \left(\Gamma_{1/2}^- \right)^2 + \text{h.c.} \right],$$

along with the other off-diagonal interaction terms. Meanwhile, we should be careful about the signs that emerge in the amplitudes resulting from the exchange of fermions along the y -axis. In our work, given that both N and $N^{(\text{h})}$ are even, like the case shown in Fig. 5(b)→(c), an additional prefactor $(-1)^{N-N^{(\text{h})}} = +1$ in the amplitude has no effect.

IV. NUMERICAL RESULTS

To analyze the groundstate properties of CS, we implement exact diagonalization (ED) on the effective model Hamiltonian H_e^{CS} . The Hilbert space bases are fully labeled by the color set $\{c\}$ of CPs for all rows, the corresponding spin-field

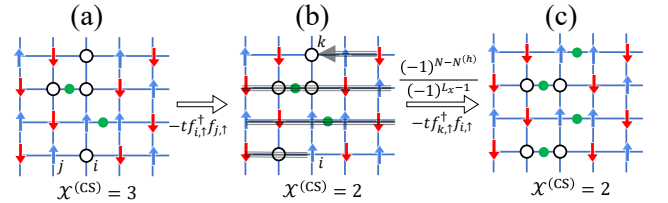


FIG. 5. Schematic images illustrate the configurations of CPs in the AF background. (a)→(b) shows a translation step of CS from the location (a) $\chi^{(\text{CS})} = 3$ to (b) $\chi^{(\text{CS})} = 2$ via the hole hopping from site- i to j in row-1. (b)→(c) shows a change of the sign of the transition amplitude when the hole hops from site- k to i . The gray arrow in (b) indicates 1D path for computing the sign.

set $\{\Gamma^z\}$, and the location $\mathcal{X}^{(\text{CS})}$ of CS, i.e.,

$$| \{c\}, \{\Gamma^z\}, \mathcal{X}^{(\text{CS})} \rangle = \left(\bigotimes_{y=1}^{L_y} |c_y\rangle \right) \left(\bigotimes_{y=1}^{L_y} | \Gamma_{\bar{y}}^z \rangle \right) | \mathcal{X}^{(\text{CS})} \rangle .$$

For example, the string configuration depicted in Fig. 2(d) is labeled as $\{c\} = \{\mathbf{g}, \mathbf{g}, \mathbf{g}, \mathbf{r}, \mathbf{b}, \mathbf{b}, \mathbf{r}, \mathbf{g}\}$, $\{\Gamma^z\} = \{2, 0, -3, 2, -4, 2, -1, 2\}$, and $\mathcal{X}^{(\text{CS})} = 3$. The absolute values of spin fields are capped at $| \Gamma_{\bar{y}}^z | \leq 8$. and the equalities $\sum_{y=1}^{L_y} n_y^{\mathbf{r}} = \sum_{y=1}^{L_y} n_y^{\mathbf{b}}$ and $\sum_y \Gamma_{\bar{y}}^z = 0$ hold. And thus, for $L_x = 11$ and $L_y = 6$, the size of the Hilbert space reaches up to 18,601,989. The wave function can be spanned as a superposition

$$| \psi \rangle = \sum_{\{c\}, \{\Gamma^z\}, \mathcal{X}^{(\text{CS})}} \psi \left(\{c\}, \{\Gamma^z\}, \mathcal{X}^{(\text{CS})} \right) | \{c\}, \{\Gamma^z\}, \mathcal{X}^{(\text{CS})} \rangle .$$

The brutal force of 2D DMRG method is also employed to investigate the CS motion in the t - J_z model (1). Unless otherwise stated, we set the bond dimension $\chi = 8,192$ to ensure truncation errors below 10^{-5} for a cylinder with $L_x \leq 23$ and $L_y = 6$ (App. 2). We choose two distinct strengths for the Ising-type interaction $J_z = 0.6$ and 1, where a π -phase string is favored in the ground state. In addition, we adjust J_z twice for bonds connected to sites at two edge columns to prevent the formation of a frozen string.

A. Hole-density distribution

For a cylinder with a finite length, the hole-density distribution provides a signal of CS [3, 7]. As illustrated in the upper panel of Fig. 6, with defining the local hole density $n^{(\text{h})}(x, y) = \langle 1 - n_{\uparrow}(x, y) - n_{\downarrow}(x, y) \rangle$ at site- $i = (x, y)$, we get the average hole density

$$\bar{n}^{(\text{h})}(x) = \frac{1}{L_y} \sum_{y=1}^{L_y} n^{(\text{h})}(x, y),$$

which indicates that holes tend to congregate at the cylinder center. Similarly, with the local magnetic moment $m^z(x, y) = (1/2) \langle n_{\uparrow}(x, y) - n_{\downarrow}(x, y) \rangle$, we compute the average magnetic moment

$$\bar{m}^z(x) = \frac{1}{L_y} \sum_{y=1}^{L_y} (-1)^{x+y} m^z(x, y)$$

in the lower panel of Fig. 6, showing a clear π -phase shift in the AF background. At large $J_z = 1$, the effective model demonstrates a semi-quantitative agreement with the DMRG numerical results, thereby providing strong support for the CS picture. In comparison, the DMRG result at $J_z = 0.6$ shows that the hole-density pack becomes slightly broader.

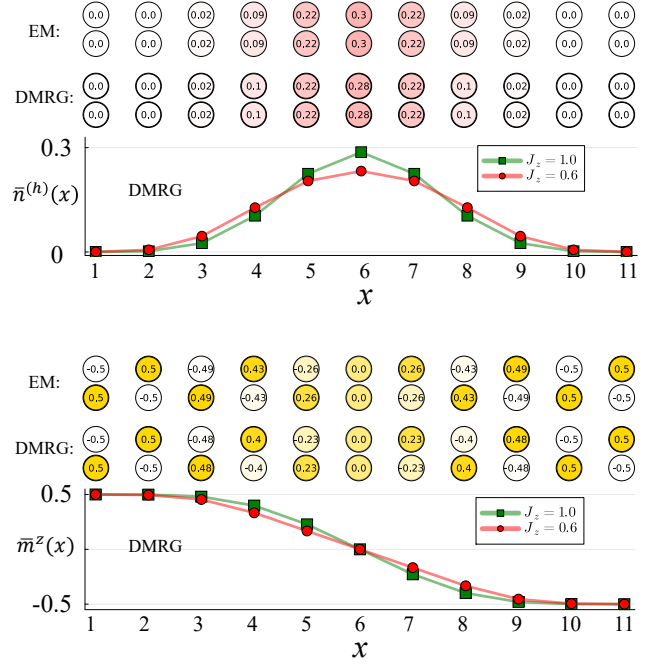


FIG. 6. The distribution of the hole density (upper panel) and magnetic moment (lower panel) in a 11×6 cylinder. The values of the local hole density $n^{(\text{h})}(x, y)$ and the local magnetic moment $m^z(x, y)$ are written in the circles, which denote the lattice sites in row-1 and row-2. A comparison is made between the ED results of the effective model (3) and the DMRG results of the t - J_z model (1) at $J_z = 1$. The average hole density $\bar{n}^{(\text{h})}(x)$ and the average magnetic moment $\bar{m}^z(x)$ calculated by 2D-DMRG are also plotted as a function of x -coordinate at $J_z = 1$ (green square) and 0.6 (red circle).

B. Spectra of spin fields

In any given row- \bar{y} , the spin field $\Gamma_{\bar{y}}^z$ displays statistical features in the reduced density matrix

$$\begin{aligned} \rho_{\bar{y}} &= \text{tr}_p | \psi \rangle \langle \psi | \\ &= \sum_{c_y, c_{y+1}, \Gamma_{\bar{y}}^z} \Lambda(c_y, c_{y+1}, \Gamma_{\bar{y}}^z) |c_y c_{y+1}\rangle | \Gamma_{\bar{y}}^z \rangle \langle \Gamma_{\bar{y}}^z | \langle c_y c_{y+1} | \end{aligned}$$

after other degrees of freedom p are traced out. The resulting spectrum weight Λ is referred to as the *fingerprint* of CS. We notice that the spectrum is independent on the choice of \bar{y} owing to the translation symmetry along the y -axis, so we simplify the definition to $\Lambda(c, c', \Gamma^z) \equiv \Lambda(c_y, c_{y+1}, \Gamma_{\bar{y}}^z)$, where both c and c' represent color values.

The statistical features are summarized below: (i) For channels $\mathbf{r-g}$ and $\mathbf{b-g}$, spectrum weights primarily distribute at $\Gamma^z = \pm 1$ and ± 3 , while $\mathbf{r-b}$ shows concentration at $\Gamma^z = \pm 2$ (Fig. 7(a-d)). Remarkably, this phenomenon persists even at a lower value of $J_z = 0.6$ (Fig. 7(e,f)). The concentration of the spectrum weight at $\Gamma^z = \pm 2$ for $\mathbf{r-b}$ suggests the confinement of spinon and dual-hole. (ii) Additionally, deviations from the effective theory are noticeable in the spectra for $\mathbf{r-g}$ and $\mathbf{b-g}$ (Fig. 7(c,e)). In comparison to $\mathbf{b-g}$, the increased weight

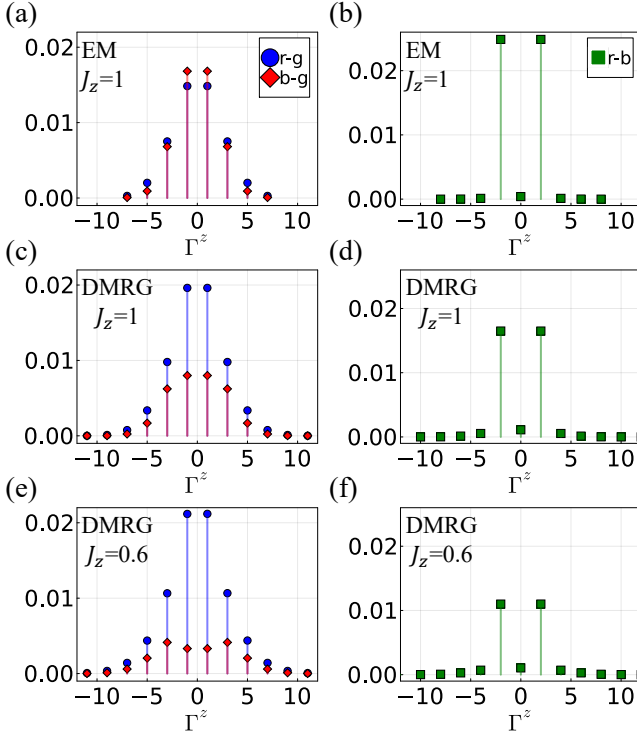


FIG. 7. The spectrum weight $\Lambda(c, c', \Gamma^z)$ as a function of the spin field Γ^z in a 11×6 cylinder at (a-d) $J_z = 1$ and (e,f) 0.6. Both the channels (a,c,e) **r-g** and **b-g**, as well as (b,d,f) **r-b**, are investigated. A comparison is made between (a,b) the ED results of the effective model (3), and (c-f) the DMRG results of the t - J_z model (1).

for **r-g** implies higher spinon mobility compared to dual-hole. This is reasonable because the **r-g** channel uses the bases with $\Gamma^z = \pm 1$ (Fig. 4(a,b)). (iii) When considering the exchanging process between **b** and **g** in the off-diagonal interaction $H_0^{(b-g/g-b)}$, the spectrum weight for **b-g** reaches its maximum values at $\Gamma^z = \pm 3$, showcasing two peaks when $J_z = 0.6$ (Fig. 4(e)). This indicates that CS exhibits larger quantum fluctuations and is more “soft” at small J_z . However, these peaks vanish due to the dominant H_d at large J_z (Fig. 4(a,c)).

C. Wave packs

We have demonstrated the existence of CS and elucidated its movement, akin to the movement of strings in frustrated systems [22, 25, 37]. It is important to note that such dimensionality reduction is not a result of the aspect ratio chosen in 2D DMRG. Even with larger L_y , the result is in good agreement with the effective model (see App. 3). As the string approaches the edge columns, it can “feel” the repulsion interactions, particularly when the distance is shorter than the characteristic distance d_{ec} . This phenomenon is analog to the entropy-reduced force observed at finite temperatures [38].

To simplify, we treat CS as a “hardcore” particle with a finite core radius of $L_s/2$, which could be smaller than d_{ec} . For the lowest-energy translation mode, the distribution of the

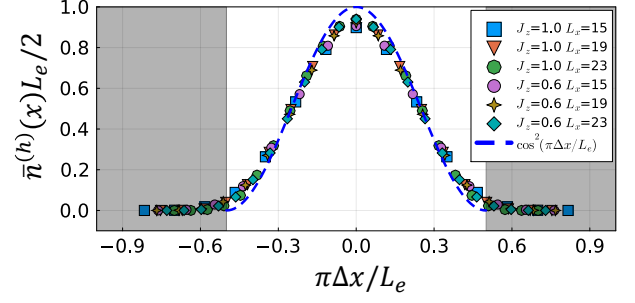


FIG. 8. The rescaled average hole density in a $L_x \times 6$ cylinder with the length $L_x = 15, 19, 23$, as calculated by 2D DMRG, is presented as a function of the rescaled displacement in the t - J_z model at $J_z = 1$ and 0.6. The gray area indicates boundary-interactive regions. The blue dashed line gives a function of $\cos^2(\pi \Delta x / L_e)$ in the white area.

average hole density is readily derived as

$$\bar{n}^{(h)}(x) = \frac{2}{L_e} \cos^2\left(\frac{\pi \Delta x}{L_e}\right),$$

where $\Delta x = x - x_c$ represents the displacement from the center $x_c = (L_x + 1)/2$, and $L_e = L_x - L_s$ is the effective length for the CS motion. After rescaling, as shown in Fig. 8, the curves $\bar{n}^{(h)}(x)$ at different values of L_x and J_z can be collapsed onto a single curve with a tunable parameter L_e .

From the CS scenario, we can immediately propose a scaling ansatz for the groundstate energy of a CS in the AF background, i.e.,

$$E = -NJ_z - 2t_s \cos\left(\frac{\pi}{L_e}\right) + \beta(L_y),$$

where the first leading term signifies the energy contribution from the AF background, the second term represents the kinetic energy arising from the translation of CS characterized by an effective hopping amplitude t_s , and the last term accounts for the internal energy associated with the vibration of CS dependent of L_y .

To validate the ansatz, we use 2D DMRG to compute the groundstate energy at different values of L_x when $L_y = 6$. In Fig. 9, after subtracting the leading term, the residual energy manifests an excellent function of $\cos(\pi/L_e)$. Correspondingly, the core radii are around 3.5 at $J_z = 1$ with slight discrepancies, which is close to the predicted $L_y/2 = 3$ by Zaanen. At lower J_z , the increased core radius reflects the softening of the CS. Most importantly, the effective hopping amplitude t_s can be extracted from the energy scaling, and its magnitude is ~ 0.1 which is strikingly close to the energy scale of the room temperature when considering the recognized model parameters for cuprates [39].

D. Pinning field

Following the Zaanen’s description, the quantum strings in cuprates are “rivers of charge” [19], or maybe alternatively

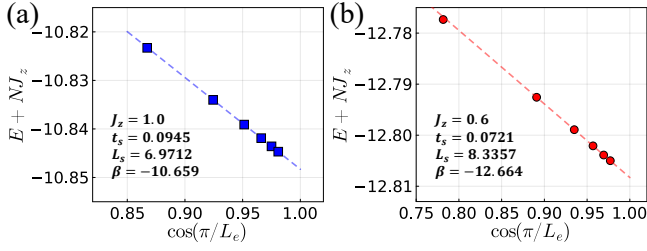


FIG. 9. The residual energy of the t - J_z model calculated by 2D DMRG at (a) $J_z = 1$ and (b) 0.6 in a $L_x \times 6$ cylinder with the length $L_x = 13, \dots, 23$. Two dashed lines give the best linear fitting.

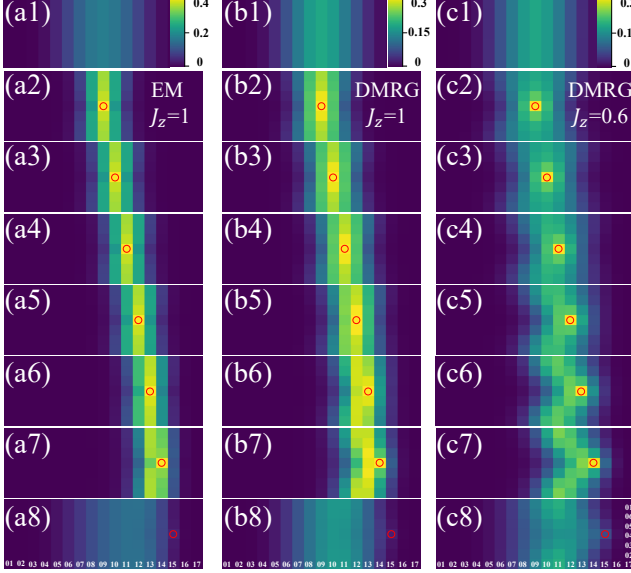


FIG. 10. The distribution of the local hole density $n^{(h)}(x, y)$ in a 17×6 cylinder, before (a1,b1,c1) and after (a2-a8,b2-b8,c2-c8) applying a pinning field with the strength $V_p = 0.5$ at different sites (red circles). A comparison is made between (a) the ED results of the effective model (3) at $J_z = 1$, and (b,c) the DMRG results of the t - J_z model (1) at (b) $J_z = 1$ and (c) 0.6.

rephrased as “holes moving in the river.” In our new scenario, three distinct CPs can move in the CS. Next, we can introduce a small pinning field $-V_p(1 - n_{i,\uparrow} - n_{i,\downarrow})$ at site- i with the field strength $V_p = 0.5$ to tweezer the CS, as shown in the second rows of Fig. 10(a-c).

As illustrated in Fig. 10, both the effective model and the t - J_z model demonstrate that the pinning field is capable of dragging CS to the vicinity of the right edge column. In these cases, the field strength is much larger than the kinetic energy of the CS, which is approximately $2t_s$. At large J_z (Fig. 10(a,b)), the CS bends when its distance from the edge column falls within the range of the characteristic distance $d_{ec} > L_s/2$, indicating a deviation from a rigid “hardcore” behavior. When the pinning field shifts to the last third x -position (Fig. 10(a8,b8,c8)), it is unable to pin the CS because the deformation energy of the CS becomes larger than the pinning energy. At smaller $J_z = 0.6$, the string can feel the edge column earlier (Fig. 10(c4)), which reflects a larger core

radius, thereby supporting the notion of the CS softening in Fig. 9.

V. CONCLUSION AND DISCUSSION

A bottom-up effective theory has been developed to explain the fully-filled striped phase of the hole-doped t - J_z model, where the quantum string in the antiferromagnetic background is colored with three distinct particles, beyond the existing description of sublattice parity order [19, 40]. Meanwhile, the colored string is also different from the conventional strings, which are designed for ultra-low doping cases [39, 41]. Furthermore, the application of a pinning field, such as the tweezer light in an optical lattice [42], enables visualization and manipulation of the quantum string. These findings are semi-quantitatively validated through the large-scale 2D-DMRG calculations.

Our effective theory may be viewed as a 1+1D gauge theory, in which color particles can interact with a $U(1)$ gauge field. Off-diagonal interactions induce vibrations in the string. The terms along the string facilitate the creation and movement of spinons and dual-holes, which is crucial for electron pairing. For example, the process $\uparrow\downarrow\uparrow \rightarrow \uparrow\downarrow\uparrow$. Therefore, our effective theory not only provides a more quantitative description of the quantum string, but also establishes a direct connection to superconductivity. Indeed, this effective theory can be readily extended to many directions, e.g., t - t' - J_z model and t - J model. Additionally, it can be used to investigate the partially-filled stripe phases. Thus, we believe that our work may lead to a significant breakthrough in the comprehension of high- T_c superconductivity mechanisms.

VI. ACKNOWLEDGEMENT

We would like to thank Hao Ding, Shi-Ping Feng, Jin Zhang, Shi-Wei Zhang, and Yuan-Yao He for many helpful discussions. This paper is also in memory of Prof. Peter Fulde and Prof. Jan Zaanen [43], who contributed a lot to the quantum strings. S. J. H. acknowledges funding from MOST Grant No. 2022YFA1402700, NSFC No. U2230402, NSFC Grant No. 12174020. X.-F. Z. acknowledges funding from the National Science Foundation of China under Grants No. 12274046, No. 11874094, No. 12147102, and No. 12347101, the Chongqing Natural Science Foundation under Grant No. CSTB2022NSCQ-JQX0018, the Fundamental Research Funds for the Central Universities Grant No. 2021CDJZYJH-003, and the Xiaomi Foundation/Xiaomi Young Talents Program.

APPENDIX

1. Phase transition

To show the transition from the hole cluster state to the string state with a π -phase shift, we use 2D DMRG to cal-

culate the energy of two low-energy states as a function of the parameter J_z . The energy values are presented in the Table A1. Then, we can find that the ground state exhibits a preference for the π -phase string state when $J_z \leq 3.8$, while the hole cluster state has a lower energy when $J_z \geq 3.9$. Therefore, we estimate that the transition point occurs at $J_{z,c} \approx 3.85$.

J_z	Hole cluster	π -phase string
3.5	-235.3558981	-235.6769177
3.6	-241.8920491	-242.1266182
3.7	-248.4342094	-248.5815498
3.8	-254.9844699	-255.0416582
3.9	-261.5423043	-261.5068928
4	-268.1071546	-267.9772034

TABLE A1. The energy values for two competing states calculated by 2D DMRG with the bond dimension $\chi = 2,048$.

2. 2D-DMRG benchmark for $L_y = 6$

We show the truncation errors at different values of cylinder length L_x and bond dimension χ when $L_y = 6$ in Table A2, as the cylinder is partitioned into two equal-size segments in 2D DMRG. We find that $\chi = 8,192$ can ensure the truncation errors below 10^{-5} . Moreover, the benchmark of the groundstate energy values is shown in Table A3, and the relative energy difference between $\chi = 4,096$ and $8,192$ is $\sim 10^{-5}$.

$J_z = 0.6$			
L_x	χ		
	2,048	4,096	8,192
11	1.28×10^{-4}	4.28×10^{-5}	9.95×10^{-6}
13	1.13×10^{-4}	3.77×10^{-5}	8.91×10^{-6}
15	9.21×10^{-5}	3.11×10^{-5}	7.34×10^{-6}
17	7.77×10^{-5}	2.57×10^{-5}	5.98×10^{-6}
19	6.57×10^{-5}	2.13×10^{-5}	4.99×10^{-6}
21	5.60×10^{-5}	1.81×10^{-5}	4.26×10^{-6}
23	4.89×10^{-5}	1.61×10^{-5}	3.70×10^{-6}
$J_z = 1$			
L_x	χ		
	2,048	4,096	8,192
11	2.39×10^{-5}	5.10×10^{-6}	6.41×10^{-7}
13	1.87×10^{-5}	4.01×10^{-6}	5.08×10^{-7}
15	1.48×10^{-5}	3.16×10^{-6}	4.00×10^{-7}
17	1.21×10^{-5}	2.57×10^{-6}	3.26×10^{-7}
19	1.02×10^{-5}	2.17×10^{-6}	2.74×10^{-7}
21	8.77×10^{-6}	1.87×10^{-6}	2.36×10^{-7}
23	7.84×10^{-6}	1.64×10^{-6}	2.08×10^{-7}

TABLE A2. The truncation errors in 2D DMRG.

3. A larger cylinder with $L_y = 8$

To show the size effect caused by the finite circumference L_y , we consider a larger cylinder with $L_y = 8$. After truncating the effective spin field to $|\Gamma^z| \leq 6$, the resulting Hilbert space

$J_z = 0.6$			
L_x	χ		
	2,048	4,096	8,192
11	-52.31128073	-52.32675360	-52.33120591
13	-59.55409964	-59.57201159	-59.57733794
15	-66.76720764	-66.78673057	-66.79257242
17	-73.97240347	-73.99274493	-73.99891747
19	-81.17485452	-81.19577544	-81.20208757
21	-88.37617798	-88.39740626	-88.40388350
23	-95.57700851	-95.59849368	-95.60499496
$J_z = 1$			
L_x	χ		
	2,048	4,096	8,192
11	-76.79074819	-76.79444193	-76.79506575
13	-88.81843623	-88.82257977	-88.82329538
15	-100.8289033	-100.8332598	-100.8340180
17	-112.8338499	-112.8383246	-112.8391054
19	-124.8365616	-124.8411020	-124.8418960
21	-136.8381993	-136.8427837	-136.8435863
23	-148.8392695	-148.8438775	-148.8446859

TABLE A3. The groundstate energy calculated by 2D DMRG.

dimension is approximately $1,522,307,837 \approx 1.4G$, which is notably large. Due to the limitations of computer memory, we restrict $|\Gamma_{ij}^z| \leq 4$ in the effective model (3). As shown in Fig. S1, both the distribution of the average hole density and magnetic moment demonstrate that the ED results from the effective model still match well with the DMRG results from the t - J_z model, when the bond dimension $\chi = 12,288$ is adopted. Moreover, as shown in Fig. S2, the spectra of the spin fields for $L_y = 8$ also display the same features as the one for $L_y = 6$.

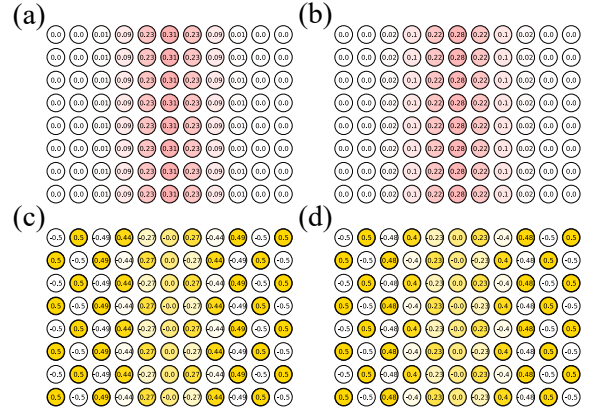


FIG. S1. The distribution of (a,b) the local hole density $n^{(h)}(x, y)$ and (c,d) the local magnetic moment $m^z(x, y)$ in a 11×8 cylinder at $J_z = 1$. Their values are written in circles denoting the lattice sites in all rows. A comparison is made between (a,c) the ED results of the effective model (3) and (b,d) the DMRG results of the t - J_z model (1).

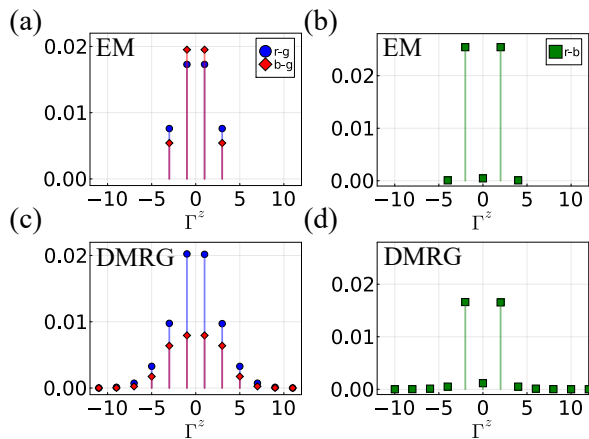


FIG. S2. The spectrum weight $\Lambda(c, c', \Gamma^z)$ as a function of the spin field Γ^z in a 11×8 cylinder at $J_z = 1$. Both the channels (a,b) **r-g** and **b-g**, as well as (c,d) **r-b**, are investigated. A comparison is made between (a,c) the ED results of the effective model (3), and (b,d) the DMRG results of the t - J_z model (1).

-
- [1] M. A. Kastner, R. J. Birgeneau, G. Shirane, and Y. Endoh, “Magnetic, transport, and optical properties of monolayer copper oxides,” *Reviews of Modern Physics* **70**, 897–928 (1998).
- [2] Patrick A. Lee, Naoto Nagaosa, and Xiao-Gang Wen, “Doping a mott insulator: Physics of high-temperature superconductivity,” *Rev. Mod. Phys.* **78**, 17 (2006).
- [3] B. Zheng, Chia-Min Chung, Philippe Corboz, Georg Ehlers, Mingpu Qin, Reinhard M. Noack, Hao Shi, Steven R. White, Shiwei Zhang, and Garnet Kin-Lic Chan, “Stripe order in the underdoped region of the two-dimensional hubbard model,” *Science* **358**, 1155 – 1160 (2016).
- [4] Qiaoyi Li, Yuan Gao, Yuan-Yao He, Yang Qi, Bin-Bin Chen, and Wei Li, “Tangent space approach for thermal tensor network simulations of the 2d hubbard model,” *Phys. Rev. Lett.* **130**, 226502 (2023).
- [5] Alexander Wietek, Yuan-Yao He, Steven R. White, Antoine Georges, and E. Miles Stoudenmire, “Stripes, antiferromagnetism, and the pseudogap in the doped hubbard model at finite temperature,” *Phys. Rev. X* **11**, 031007 (2021).
- [6] Shoushu Gong, W. Zhu, and D. N. Sheng, “Robust d -wave superconductivity in the square-lattice t - j model,” *Physical Review Letters* **127**, 097003 (2021).
- [7] Yi-Fan Jiang, Jan Zaanen, Thomas P. Devereaux, and Hong-Chen Jiang, “Ground state phase diagram of the doped hubbard model on the four-leg cylinder,” *Phys. Rev. Res.* **2**, 033073 (2020).
- [8] Chia-Min Chung, Mingpu Qin, Shiwei Zhang, Ulrich Schollwöck, and Steven R. White (The Simons Collaboration on the Many-Electron Problem), “Plaquette versus ordinary d -wave pairing in the t' -hubbard model on a width-4 cylinder,” *Phys. Rev. B* **102**, 041106 (2020).
- [9] Xin Lu, Feng Chen, W. Zhu, D. N. Sheng, and Shou-Shu Gong, “Emergent superconductivity and competing charge orders in hole-doped square-lattice t - j model,” *Phys. Rev. Lett.* **132**, 066002 (2024).
- [10] Yi-Fan Jiang, Thomas P. Devereaux, and Hong-Chen Jiang, “Ground-state phase diagram and superconductivity of the doped hubbard model on six-leg square cylinders,” *Phys. Rev. B* **109**, 085121 (2024).
- [11] Hong-Chen Jiang and Thomas P. Devereaux, “Superconductivity in the doped hubbard model and its interplay with next-nearest hopping t' ,” *Science* **365**, 1424–1428 (2019).
- [12] Hao Xu, Chia-Min Chung, Mingpu Qin, Ulrich Schollwöck, Steven R. White, and Shiwei Zhang, “Coexistence of superconductivity with partially filled stripes in the hubbard model,” *Science* **384**, eadh7691 (2024), <https://www.science.org/doi/pdf/10.1126/science.adh7691>.
- [13] Eduardo Fradkin, Steven A. Kivelson, and John M. Tranquada, “Colloquium: Theory of intertwined orders in high temperature superconductors,” *Rev. Mod. Phys.* **87**, 457–482 (2015).
- [14] John M. Tranquada, “Spins, stripes, and superconductivity in hole-doped cuprates,” in *AIP Conference Proceedings* (AIP, 2013).
- [15] H. A. Mook, Pengcheng Dai, F. Dogan, and R. D. Hunt, “One-dimensional nature of the magnetic fluctuations in $\text{YBa}_2\text{Cu}_3\text{O}_{6.6}$,” *Nature (London)* **404**, 729–731 (2000), [arXiv:cond-mat/0004362 \[cond-mat.supr-con\]](https://arxiv.org/abs/cond-mat/0004362).
- [16] Zengyi Du, Hui Li, Sang Hyun Joo, Elizabeth P. Donoway, Jinho Lee, J. C. Séamus Davis, Genda Gu, Peter D. Johnson, and Kazuhiro Fujita, “Imaging the energy gap modulations of the cuprate pair-density-wave state,” *Nature (London)* **580**, 65–70 (2020), [arXiv:2109.14033 \[cond-mat.supr-con\]](https://arxiv.org/abs/2109.14033).
- [17] Steven R. White and D. J. Scalapino, “Energetics of domain walls in the 2d t - j model,” *Phys. Rev. Lett.* **81**, 3227–3230 (1998).
- [18] J. Zaanen, “Order out of disorder in a gas of elastic quantum strings in $2 + 1$ dimensions,” *Phys. Rev. Lett.* **84**, 753–756 (2000).

- [19] J. Zaanen, O. Y. Osman, H. V. Kruis, Z. Nussinov, and J. Tworzydło, “The geometric order of stripes and Luttinger liquids,” *Philosophical Magazine, Part B* **81**, 1485–1531 (2001), [arXiv:cond-mat/0102103 \[cond-mat.str-el\]](#).
- [20] Yoshihiro Nishiyama, “Quantum-fluctuation-induced collisions and subsequent excitation gap of an elastic string between walls,” *Phys. Rev. B* **66**, 184501 (2002).
- [21] P. Fulde and F. Pollmann, “Strings in strongly correlated electron systems,” *Annalen der Physik* **520**, 441–449 (2008), [arXiv:0711.2129 \[cond-mat.str-el\]](#).
- [22] Xue-Feng Zhang and Sebastian Eggert, “Chiral edge states and fractional charge separation in a system of interacting bosons on a kagome lattice,” *Phys. Rev. Lett.* **111**, 147201 (2013).
- [23] Xue-Feng Zhang, Yin-Chen He, Sebastian Eggert, Roderich Moessner, and Frank Pollmann, “Continuous easy-plane deconfined phase transition on the kagome lattice,” *Phys. Rev. Lett.* **120**, 115702 (2018).
- [24] Dong-Xu Liu, Zijian Xiong, Yining Xu, and Xue-Feng Zhang, “Deconfined quantum phase transition on the kagome lattice: Distinct velocities of spinon and string excitations,” *Phys. Rev. B* **109**, L140404 (2024).
- [25] Zheng Zhou, Changle Liu, Zheng Yan, Yan Chen, and Xue-Feng Zhang, “Quantum dynamics of topological strings in a frustrated Ising antiferromagnet,” *npj Quantum Materials* **7**, 60 (2022), [arXiv:2010.01750 \[cond-mat.str-el\]](#).
- [26] Zheng Zhou, Changle Liu, Dong-Xu Liu, Zheng Yan, Yan Chen, and Xue-Feng Zhang, “Quantum tricriticality of incommensurate phase induced by quantum strings in frustrated Ising magnetism,” *SciPost Physics* **14**, 037 (2023), [arXiv:2005.11133 \[cond-mat.str-el\]](#).
- [27] Zheng Zhou, Zheng Yan, Changle Liu, Yan Chen, and Xue-Feng Zhang, “Quantum simulation of two-dimensional U(1) gauge theory in rydberg atom arrays,” (2022), [arXiv:2212.10863 \[quant-ph\]](#).
- [28] Yuan Wan and Oleg Tchernyshyov, “Quantum strings in quantum spin ice,” *Phys. Rev. Lett.* **108**, 247210 (2012).
- [29] Xue-Feng Zhang, Shijie Hu, Axel Pelster, and Sebastian Eggert, “Quantum domain walls induce incommensurate supersolid phase on the anisotropic triangular lattice,” *Phys. Rev. Lett.* **117**, 193201 (2016).
- [30] John McGreevy, “Generalized Symmetries in Condensed Matter,” *Annual Review of Condensed Matter Physics* **14**, 57–82 (2023), [arXiv:2204.03045 \[cond-mat.str-el\]](#).
- [31] Zijian Xiong, “1-form symmetry and the selection rule of the plaquette valence bond solid phase on the kagome lattice,” *Phys. Rev. B* **108**, 195107 (2023).
- [32] Nabil Iqbal and John McGreevy, “Mean string field theory: Landau-Ginzburg theory for 1-form symmetries,” *SciPost Phys.* **13**, 114 (2022).
- [33] Yosuke Nagaoka, “Ferromagnetism in a narrow, almost half-filled s band,” *Phys. Rev.* **147**, 392–405 (1966).
- [34] Hal Tasaki, “Extension of nagaoka’s theorem on the large- u hubbard model,” *Phys. Rev. B* **40**, 9192–9193 (1989).
- [35] Wei Chen, Kazuo Hida, and B. C. Sanctuary, “Ground-state phase diagram of $s = 1$ XXZ chains with uniaxial single-ion-type anisotropy,” *Phys. Rev. B* **67**, 104401 (2003).
- [36] Zijian Xiong, Yining Xu, and Xue-Feng Zhang, “Dynamics in the planar pyrochlore lattice: bow-tie flat band and mixed ’t Hooft anomaly,” *arXiv e-prints*, [arXiv:2111.11445 \(2021\)](#), [arXiv:2111.11445 \[cond-mat.str-el\]](#).
- [37] Xue-Feng Zhang, Shijie Hu, Axel Pelster, and Sebastian Eggert, “Quantum domain walls induce incommensurate supersolid phase on the anisotropic triangular lattice,” *Phys. Rev. Lett.* **117**, 193201 (2016).
- [38] R. J. Baxter, [Exactly solved models in statistical mechanics](#) (Dover Publications, INC. Mineola, New York, 1982).
- [39] Elbio Dagotto, “Correlated electrons in high-temperature superconductors,” *Rev. Mod. Phys.* **66**, 763 (1994).
- [40] Fabian Grusdt and Lode Pollet, “ z_2 parton phases in the mixed-dimensional $t - J_z$ model,” *Phys. Rev. Lett.* **125**, 256401 (2020).
- [41] D. N. Sheng, Y. C. Chen, and Z. Y. Weng, “Phase string effect in a doped antiferromagnet,” *Phys. Rev. Lett.* **77**, 5102–5105 (1996).
- [42] Aaron W. Young, William J. Eckner, Nathan Schine, Andrew M. Childs, and Adam M. Kaufman, “Tweezer-programmable 2d quantum walks in a hubbard-regime lattice,” *Science* **377**, 885 (2022).
- [43] Philip W. Phillips, “The smoke of zaanen,” (2024), [arXiv:2402.00577 \[physics.hist-ph\]](#).